Infrared reflectivity of the solid solutions $LaNi_{1-x}Fe_xO_3$ $(0.00 \leqslant x \leqslant 1.00)$

Néstor E. Massa
Laboratorio Nacional de Investigación y Servicios en Espectroscopía Optica, Centro CEQUINOR, Departamento de Química y Departamento de Física, Universidad Nacional de La Plata, Casilla de Correo 962, 1900 La Plata, Argentina

Horacio Falcón
Instituto de Investigaciones en Fisicoquímica de Córdoba, Departamento de Fisicoquímica, Facultad de Ciencias Químicas, Universidad Nacional de Córdoba, Agencia Postal 4, Casilla de Correo 61, 5000 Córdoba, Argentina

Horacio Salva
Laboratorio de Resonancias Magnéticas, Centro Atómico Bariloche, 8400 Bariloche, Rio Negro, Argentina

Raúl E. Carbonio
Instituto de Investigaciones en Fisicoquímica de Córdoba, Departamento de Fisicoquímica, Facultad de Ciencias Químicas, Universidad Nacional de Córdoba, Agencia Postal 4, Casilla de Correo 61, 5000 Córdoba, Argentina

(Received 23 January 1997; revised manuscript received 19 June 1997)

We report temperature-dependent far- and midinfrared reflectivity spectra of $LaNi_{(1-x)}Fe_xO_3$ $(0.00 \leqslant x \leqslant 1.00)$ solid solutions that span the passage from $LaFeO_3$, a room-temperature antiferromagnetic insulator, to $LaNiO_3$, a known metal oxide. Light Ni doping creates defects that induce extra bands assigned to electronic transitions within the insulating gap. An incipient Drude term emerges in the reflectivity spectrum of $LaNi_{0.39}Fe_{0.61}O_3$ together with subbands that contribute to the electronic background. At these concentrations the dielectric response shows a picture in which the spectral weigh switches over toward far-infrared frequencies while phonon features develop strong antiresonances near longitudinal-optical modes. Further increment of carriers produces phonon screening and the development of a reflectivity tail that extends beyond 1 eV. We assign extra-non-Drude terms in the $700-4000\ cm^{-1}$ frequency region to transitions due to intrinsic defects. While the increment in reflectivity at far-infrared frequencies is evident for Fe concentrations well above the insulator-metal transition $(x \sim 0.30)$, the spectral features of a metal oxide, with phonons mostly screened, are found for $x = 0.23$. These metallic spectra show an absorption dip at $\sim 650\ cm^{-1}$ that is traced to the perovskite symmetric stretching longitudinal mode. It is evidence that electron-phonon interactions are present in our solid solutions even when their numbers of effective carriers are those of a metal. This characterization is also supported by the observation of weak reflectivity dips in $LaNiO_3$ that have a direct correspondence to longitudinal-optical mode frequencies of the insulating phases of our series. We infer that strong electron-phonon interactions play a role in the conductivity of those solid solutions and are likely related to polaron formation and carrier phonon-assisted hopping motion. This conclusion is supported by the quantitative agreement with experimental data achieved by calculation of optical conductivities using the small-polaron theory by Reik and Heese [H. G. Reik and D. Heese, J. Phys. Chem. Solids **28**, 581 (1967)]. We find our spectral analysis relevant toward understanding the infrared reflectivity of conducting oxides in general. Since $LaNiO_3$ is a three-dimensional compound we avoid the argument of misinterpreting spectral features as due to band leakages of unscreened phonons active in insulating crystal directions. [S0163-1829(97)05240-5]

INTRODUCTION

From the earliest measurements on conducting perovskites far-infrared spectroscopy has provided a powerful tool for the understanding of intrinsic properties of these singular oxides. However, the bulk of the information available is related to oxides becoming superconductors at relatively high temperatures. It means a wealth of information on a particular single item. This experimental situation promotes biased interpretations on many features that do not discriminate on how a particular spectroscopic feature may be related to an intrinsic property of the superconducting state in oxides.

It is because relatively few publications are found in the current literature[1] addressing a case intermediate between oxides superconductors and the dielectric insulator that we are motivated to study the infrared reflectivity of the solid solutions $LaNi_{(1-x)}Fe_xO_3$ in the whole range of impurity doping x. These solid solutions, in which the increment of the number of carriers is achieved by adding amounts of Ni ions quantitatively, span the passage from a room-temperature antiferromagnetic insulator, as is $LaFeO_3$, to $LaNiO_3$, a known metal oxide.

We can follow how the phonon structure yields to the freer-carrier contribution as they go through an insulator-metal transition and we may monitor infrared bands resembling some of the extra-Drude features that are also identified in the normal state of high-T_c superconductors. These are

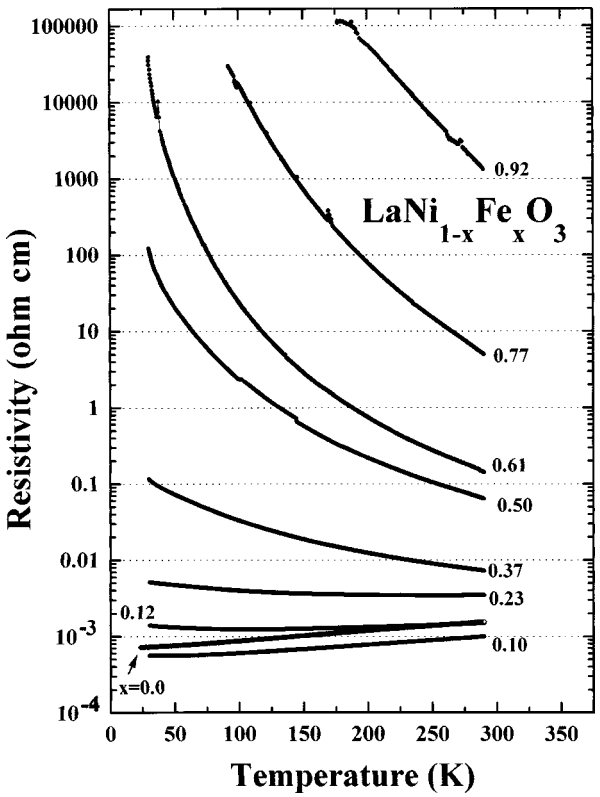

FIG. 1. Temperature dependence of the resistivities of $LaNi_{(1-x)}Fe_xO_3$ $(0.00 \leqslant x \leqslant 1.00)$.

claimed to play a principal role in explaining quasiparticle pairing.

Perovskites distort easily from the ideal cubic space group of which $SrTiO_3$ is a prototype. This compound is known to sustain quantum ferroelectricity at low temperatures and heavily doped it is a superconductor.[2] Reduced samples have infrared absorptions bands centered at about 2000 and 4000 cm^{-1} and at lower frequencies there is an absorption at 1320 cm^{-1} primarily due to oxygen defects. These may be interpreted in terms of transitions from localized levels, intraband scattering between delocalized levels,[3] or, alternatively, be assigned to a polaronic origin.[4]

SAMPLE PREPARATION AND CHARACTERIZATION

Our solid solutions, $LaNi_{(1-x)}Fe_xO_3$ $(0.0 \leqslant x \leqslant 1.0)$, are distorted perovskites. They are prepared by decomposition of the amorphous citrate precursor.[5] A concentrated solution of citric acid was added to a concentrated solution of metal nitrates until the molar ratio of citric acid to total metals was unity. The resulting solution was evaporated in a rotary evaporator at 90 °C until the precipitate acquired the consistency of a viscous syrup. The residual water was evaporated in a vacuum oven at 110 °C for 24 h. This precursor is a fine mixture of the nitrates and citric acid that after burning in air at 900 °C for 12 h was reground. The sample was then prepared by repeating this last step one more time. The pellets resulting from pressing the powder at 5 ton./cm^2 and sintered for 8 h at 1000 °C in flowing oxygen, had a glossy surface and were used in our measurements without further treatment. To verify and avoid contamination with La_2NiO_4, $LaNiO_3$ was also synthesized and sintered at 800 °C (Refs. 6, 7).

Taking into account that the oxidation states for Ni are Ni^{2+} and Ni^{3+} and that those for Fe are Fe^{3+} and Fe^{4+}, we write the general formula for our solid solutions as

$$La\{Ni^{2+}{}_m, Ni^{3+}{}_n\}\{Fe^{3+}{}_u, Fe^{4+}{}_v\}O_{3-\delta} \quad (0.00 \leqslant x \leqslant 1.00), \tag{1}$$

where $m+n=1-x$ and $u+v=x$, and where the oxygen vacancies δ are not quantified. Mössbauer spectroscopy shows that mixed oxidation states for Fe in single phase $LaNi_{0.75}Fe_{0.25}O_3$ correspond 52% to Fe^{3+} and 48% to Fe^{4+} (Ref. 8).

Rietveld refinements on x-ray diffractograms of the series $LaNi_{(1-x)}Fe_xO_3$ $(0.00 \leqslant x \leqslant 1.00)$ indicate that our samples are monophasic. Those with $x < 0.5$ have the $LaNiO_3$, i.e., rhombohedral, space group $R\mathbf{3}c$. Samples with $0.5 < x \leqslant 1$ have the orthorhombic $LaFeO_3$, $Pnma$, structure. Only for

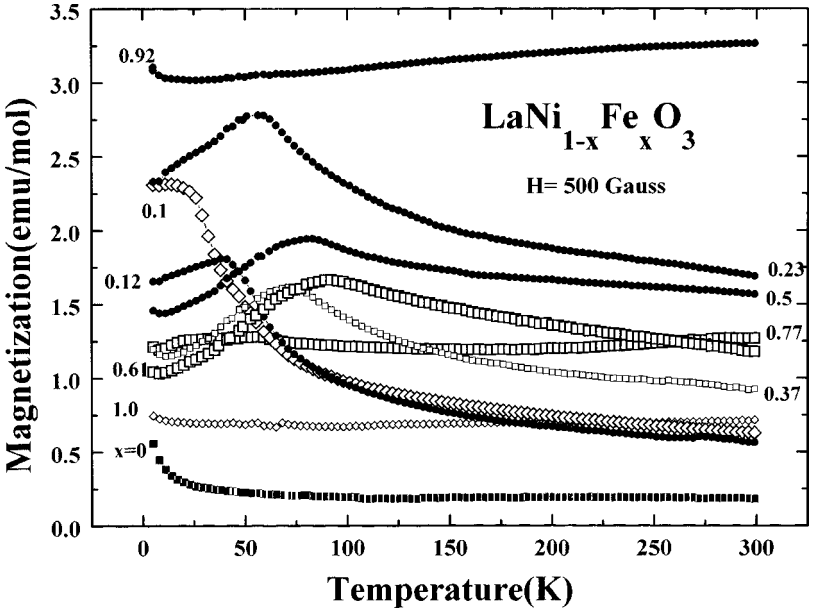

FIG. 2. Temperature dependence of the magnetic susceptibilities of $LaNi_{(1-x)}Fe_xO_3$ $(0.00 \leqslant x \leqslant 1.00)$.

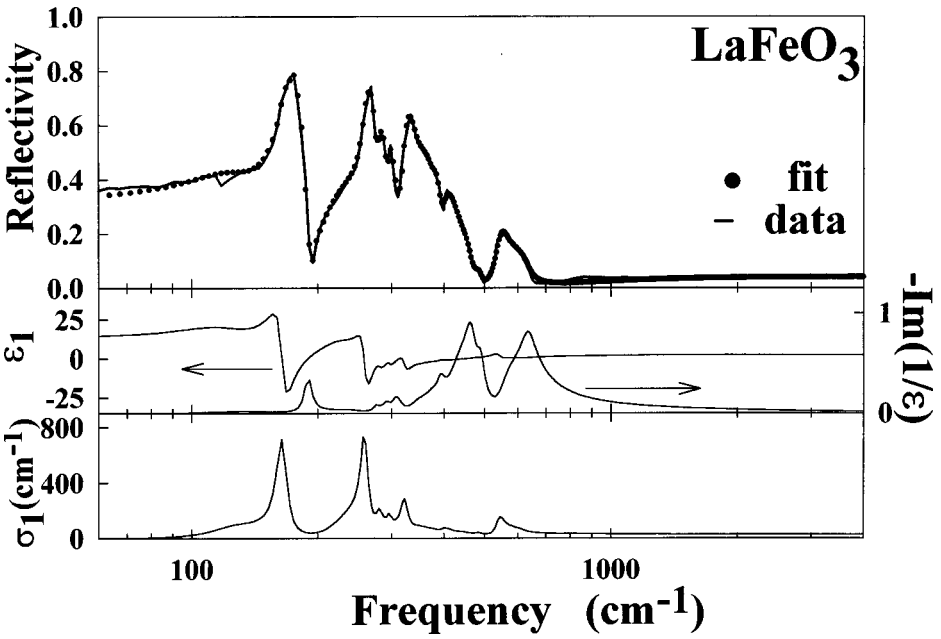

FIG. 3. Infrared reflectivity spectra; ε_1, real part of the dielectric function; $-\mathrm{Im}(1/\varepsilon)$, the imaginary part of the reciprocal of the dielectric function, and σ_1, the real part of the optical conductivity of $LaFeO_3$ at 80 K.

$LaFe_{0.50}Ni_{0.50}O_3$ both phases, orthorhombic and rhombohedral, were identified simultaneously. Cell parameters increase with Fe content and the normalized cell volume increases linearly with x due to the larger radius of Fe^{3+} (high spin) compared with Ni^{3+} (low spin). Superstructural x-rays reflections suggesting long-range order of Fe and Ni were not observed.[9]

We also characterized our samples between 4 and 300 K by four-point resistivity measurements (Fig. 1). They span nine orders of magnitude pointing to a relative simple perovskite system in which one may probe the continuous passage from a truly insulator to a metal oxide. At $x \cong 0.30$ the system exhibits an insulator-metal transition either in concentration or in temperature that, as we will discuss below, may be interpreted as consequence of gradual electron localization.

Their magnetic susceptibilities were measured with a quantum design (SQUID) magnetometer at 500 G. They are shown in Fig. 2 where the antiferromagnetic Néel transition temperature, T_N, may be deduced as a function of the iron content. These sets of measurements are in overall agreement with earlier results by Vasanthacharya *et al.*[10] and Ganguly, Vasanthacharya, and Rao.[11]

In the following paragraphs we will discuss the infrared reflectivity spectra of the solid solutions $LaNi_{(1-x)}Fe_xO_3$ with $x = 0.00$, 0.092, 0.12, 0.23, 0.37, 0.50, 0.61, 0.77, 0.90, 1.00, determined by energy-dispersion spectroscopy. Near normal reflectivity, with the pellet glued on the cold finger of an Oxford DN 1754 cryostat, has been measured at 300, 170, and 80 K from 30 to 10 000 cm^{-1} in a FTIR Bruker 113v interferometer set for 2 cm^{-1} resolution. We used a fresh surface gold mirror as a 100% reference.

Based on reflectivity features we then propose a possible interpretation for the conductivity mechanism in oxides and discuss the very good agreement with the model proposed by

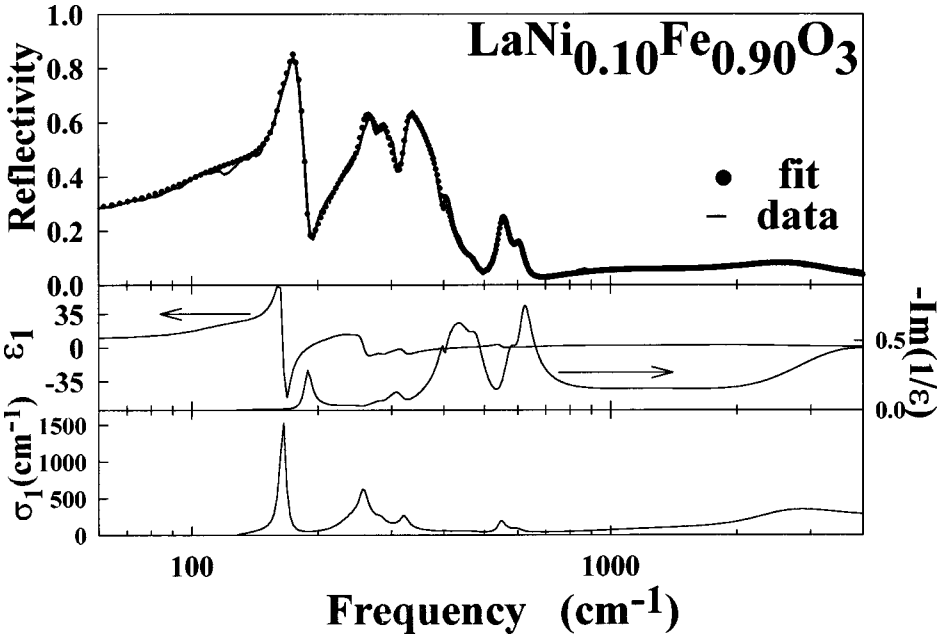

FIG. 4. Infrared reflectivity spectra; ε_1, real part of the dielectric function; $-\mathrm{Im}(1/\varepsilon)$, the imaginary part of the reciprocal of the dielectric function, and σ_1, the real part of the optical conductivity of $LaNi_{0.10}Fe_{0.90}O_3$ at 80 K.

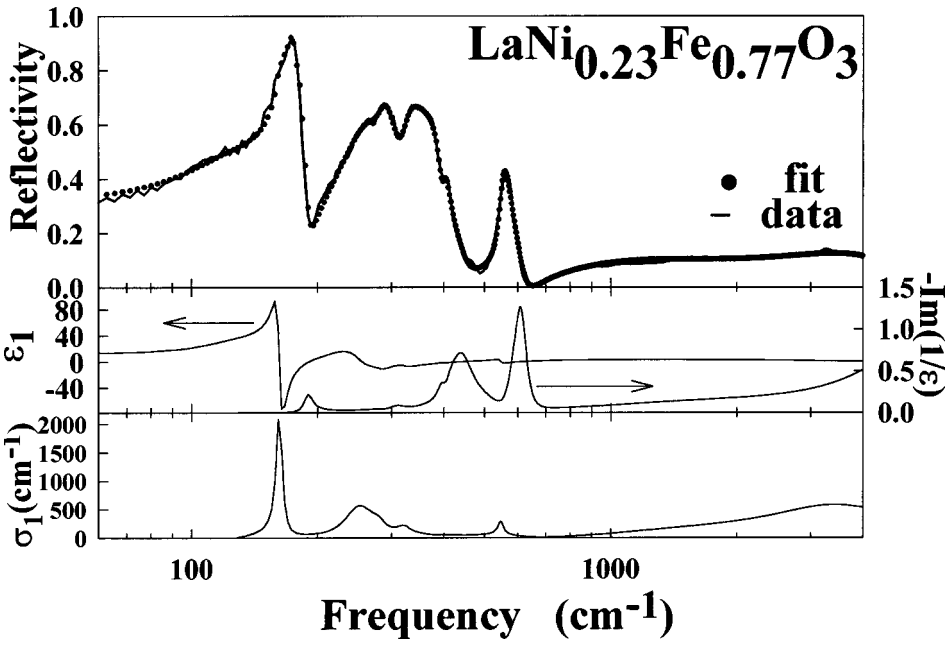

FIG. 5. Infrared reflectivity spectra; ε_1, real part of the dielectric function; $-\mathrm{Im}(1/\varepsilon)$, the imaginary part of the reciprocal of the dielectric function, and σ_1, the real part of the optical conductivity of $LaNi_{0.23}Fe_{0.77}O_3$ at 80 K.

Reik and Heese[12] for small polarons. We finish with a comment on the implication that it might have on high-T_c superconductivity.

Since we did not find evidence of structural phase transitions we will present, except when otherwise indicated, only the spectra taken at 80 K. At the studied temperatures we did not find any relation between infrared-active bands and antiferromagnetic ordering.

SPECTRAL ANALYSIS

We analyzed the spectra simulating the infrared-active features with damped Lorentzian oscillators in a classical formulation of the dielectric function.[13] Thus, $\varepsilon_{\mathrm{av}}(\omega)$, the dielectric function with uncertain weighted contributions of the lattice axes, is given by

$$\varepsilon_{\mathrm{av}}(\omega)=\varepsilon_\infty\prod_j \frac{(\Omega_{j\mathrm{LO}}^2-\omega^2+i\gamma_{j\mathrm{LO}}\omega)}{(\Omega_{j\mathrm{TO}}^2-\omega^2+i\gamma_{j\mathrm{TO}}\omega)}. \tag{2}$$

We then optimized the normal reflectivity against the experimental points and calculated the high-frequency dielectric function, ε_∞; the transverse and longitudinal jth optical frequencies, $\Omega_{j\mathrm{TO}}$ and $\Omega_{j\mathrm{LO}}$; and their transverse and longitudinal damping constants, $\gamma_{j\mathrm{TO}}$ and $\gamma_{j\mathrm{LO}}$, respectively. We also calculated the S_j strength of the jth oscillator as

$$S_j=\Omega_{j\mathrm{TO}}^{-2}\frac{(\Pi_k\Omega_{j\mathrm{LO}}^2-\Omega_{j\mathrm{TO}}^2)}{(\Pi_{k\neq j}\Omega_{k\mathrm{TO}}^2-\Omega_{j\mathrm{TO}}^2)}. \tag{3}$$

In addition, when the measured spectra required it, we added one plasma contribution (Drude term) such as

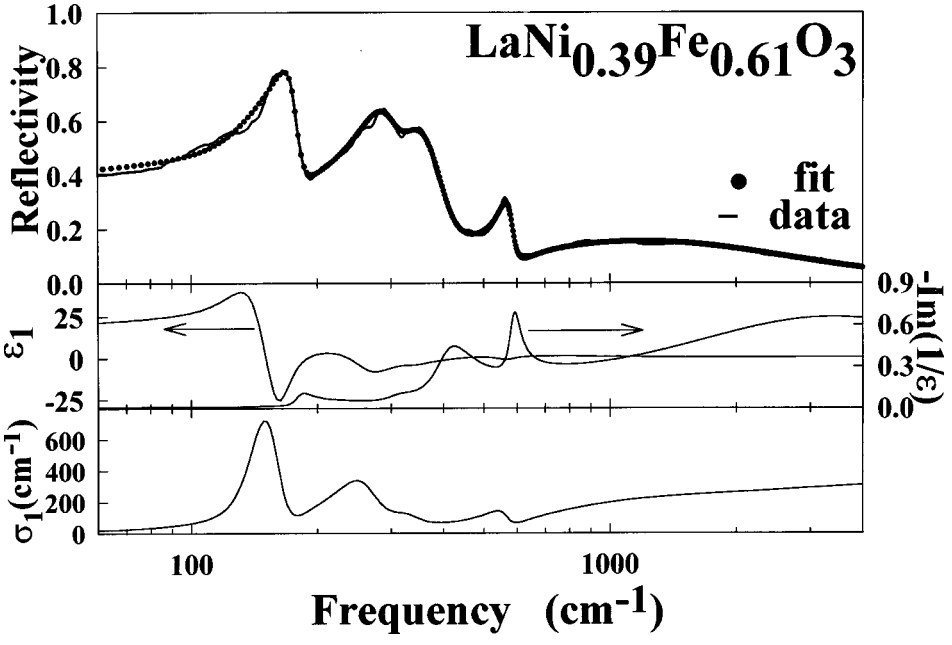

FIG. 6. Infrared reflectivity spectra; ε_1, real part of the dielectric function; $-\mathrm{Im}(1/\varepsilon)$, the imaginary part of the reciprocal of the dielectric function, and σ_1, the real part of the optical conductivity of $LaNi_{0.39}Fe_{0.61}O_3$ at 80 K.

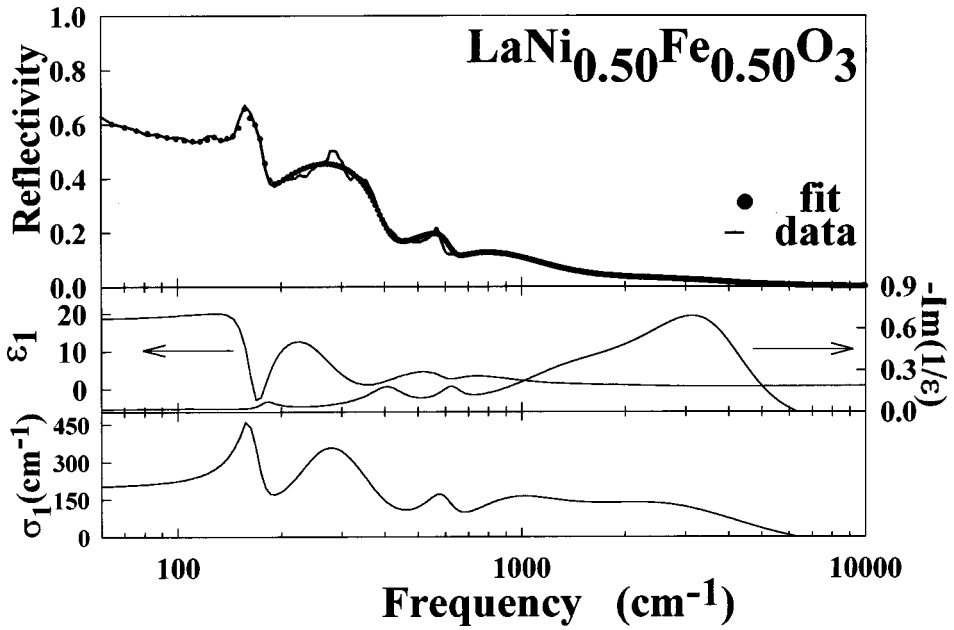

FIG. 7. Infrared reflectivity spectra; ε_1, real part of the dielectric function; $-\mathrm{Im}(1/\varepsilon)$, the imaginary part of the reciprocal of the dielectric function, and σ_1, the real part of the optical conductivity of $LaNi_{0.50}Fe_{0.50}O_3$ at 80 K.

$$-\frac{[\Omega_{\mathrm{pl}}^2+i(\gamma_p-\gamma_0)\omega]}{[\omega(\omega-i\gamma_0)]} \tag{4}$$

to the dielectric simulation function, where Ω_{pl} is the plasma frequency, γ_{pl} its damping, and γ_0 is understood as a phenomenological damping introduced by the lattice drag. When these two dampings are set equal, one retrieves the classical Drude formula.[14]

With

$$\Omega_{\mathrm{pl}}^2=4\pi e^2N/m^*, \tag{5}$$

we can estimate an effective carrier concentration $N^*=Nm/m^*$ (m and m^* are the free- and effective electron mass; N and N^* are the number and the effective number of carriers, respectively). Similar analyses using the Kramers-Kronig approach on our data yielded results in quantitative agreement with those presented here.

The reflectivities, Figs. 3–7 and 9–12 are shown together with the calculated real part of the dielectric function, ε_1; the imaginary part of the reciprocal dielectric function peaking at longitudinal modes, $-\mathrm{lm}(1/\varepsilon)$; and the real part of the optical conductivity, $\sigma_1=(\omega/4\pi)\varepsilon_2$ (ε_2 is the imaginary part of the dielectric function).

To study the optical conductivity we used theoretical expressions for small polarons due to nondiagonal phonon transitions as calculated by Reik and Heese.[12] Based on a Holstein Hamiltonian,[15] where optical properties are due to carriers in one small band, the real part of the conductivity $\sigma_1(\omega,\beta)$ for finite temperature is given by

$$\sigma_1(\omega,\beta)=\sigma_{\mathrm{DC}}\frac{\sinh(\frac{1}{2}\hbar\omega\beta)\exp[\omega^2\tau^2r(\omega)]}{\frac{1}{2}\hbar\omega\beta[1+(\omega\tau\Delta)^2]^{0.25}}, \tag{6}$$

where

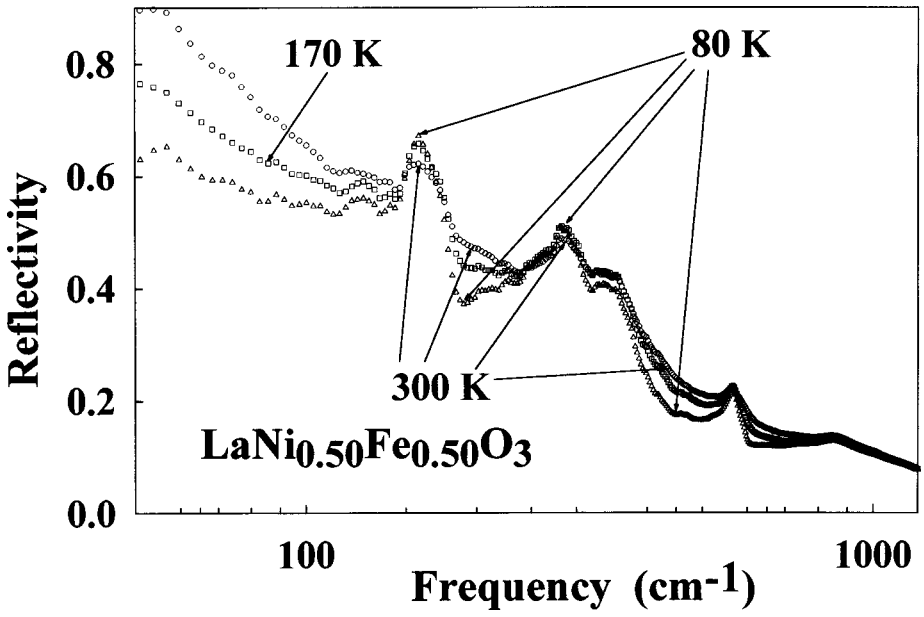

FIG. 8. Temperature dependence of the far-infrared reflectivity of $LaNi_{0.50}Fe_{0.50}O_3$ showing the effect of the electron-phonon interactions near the longitudinal-optical phonons.

TABLE I. Fitting Parameters for $LaNi_{(1-x)}Fe_xO_3$: insulators.

x	ε_∞	Ω_{to} (cm^{-1})	Ω_{lo} (cm^{-1}) Ω_{pl} (cm^{-1})	γ_{to} (cm^{-1}) γ_0 (cm^{-1})	γ_{lo} (cm^{-1}) γ_{pl} (cm^{-1})	S_j (cm^{-2})
		123.8	134.5	68.0	59.9	3.788
		164.5	189.2	11.5	8.8	3.814
		231.8	254.0	76.8	60.4	3.117
		258.9	276.4	11.7	10.6	0.51
		279.5	294.1	11.3	10.1	0.164
		295.9	309.2	8.1	22.3	0.063
		321.7	345.4	40.6	30.7	0.143
1.00	2.65	350.7	381.9	38.9	32.1	0.122
		382.7	391.7	22.7	22.2	0.006
		399.2	443.7	26.7	79.5	0.064
		454.1	462.6	38.6	32.9	0.011
		484.5	488.4	20.0	17.8	0.013
		541.1	566.0	32.6	33.7	0.133
		583.4	595.1	71.6	102.8	0.026
		621.8	630.1	50.6	42.1	0.020
		120.7	121.8	65.7	122.3	0.311
		165.2	188.6	6.1	9.42	3.008
		243.9	252.9	50.1	24.8	2.456
		256.0	282.2	14.6	16.2	0.755
		283.2	313.0	13.8	28.3	0.068
		321.4	387.3	18.4	115.4	0.249
0.90	1.14	387.7	392.9	76.2	61.9	0.003
		393.6	400.7	106.2	6.34	0.004
		401.1	445.3	5.2	116.4	0.002
		468.0	473.6	40.3	42.1	0.009
		547.0	572.4	27.8	60.7	0.099
		601.6	616.9	38.7	50.9	0.031
		801.2	849.2	961.4	1705.2	0.133
		2521.7	3014.6	1588.8	2993.8	0.466
		125.2	126.8	63.4	108.3	0.507
		162.2	189.1	6.3	11.0	4.556
		243.9	253.0	47.8	48.5	3.065
		256.0	282.2	42.3	35.0	0.947
		283.2	313.0	25.1	34.1	0.086
		321.4	387.3	29.2	414.0	0.313
		387.7	392.9	51.2	38.7	0.003
0.77	0.98	393.6	400.7	435.6	18.4	0.005
		401.1	445.3	13.9	73.9	0.002
		468.0	473.6	127.4	215.5	0.011
		547.0	572.4	21.9	87.9	0.101
		614.7	616.1	160.3	53.7	0.004
		940.7	969.2	1148.7	1917.3	0.120
		3396.3	5300.7	2801.4	4322.2	1.374
		102.7	109.2	82.9	85.8	3.292
		145.5	158.1	43.1	113.1	5.378
		161.6	180.6	33.1	17.1	0.813
		262.7	308.9	81.5	61.2	4.264
0.61	1.0	327.2	395.7	79.5	69.7	0.821
		565.7	582.0	71.36	34.3	0.294
		1015.1	1849.8	1849.8	3233.2	3.977
		1936.1	2471.9	5665.0	6039.5	0.076
			5626.7	2616.1	2616.1	

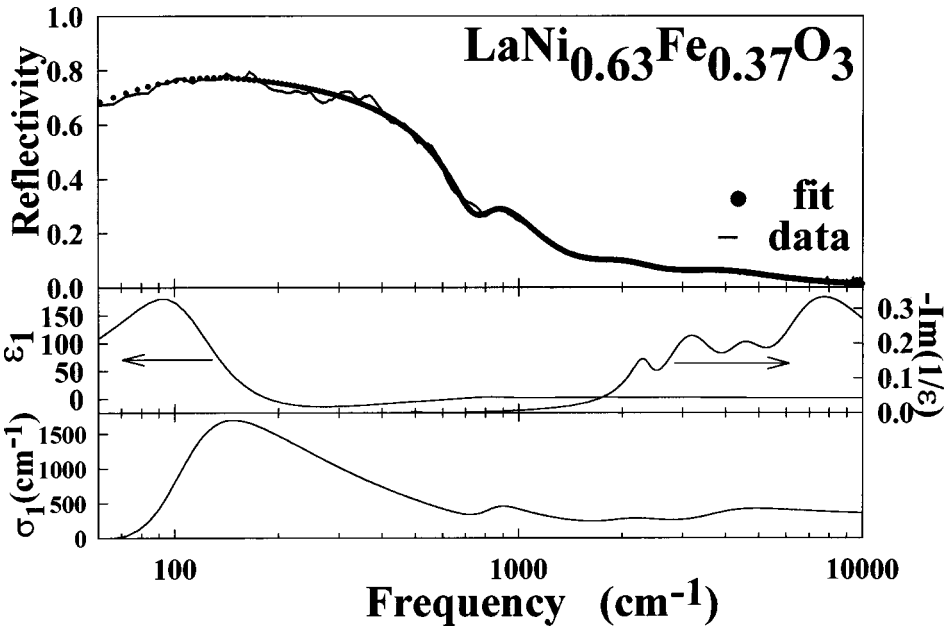

FIG. 9. Infrared reflectivity spectra; ε_1, real part of the dielectric function; $-\mathrm{Im}(1/\varepsilon)$, the imaginary part of the reciprocal of the dielectric function, and σ_1, the real part of the optical conductivity of $LaNi_{0.63}Fe_{0.37}O_3$ at 80 K.

$$r(\omega)=\left(\frac{2}{\omega\tau\Delta}\right)\ln\{\omega\tau\Delta+[1+(\omega\tau\Delta)^2]^{1/2}\}-[2/(\omega\tau\Delta)^2]\times\{[1+(\omega\tau\Delta)^2]^{1/2}-1\}, \quad (7)$$

with

$$\Delta=2\overline{\omega\tau} \quad (8)$$

and

$$\tau^2=[\sinh(\tfrac{1}{2}\hbar\overline{\omega\beta})]/2\overline{\omega^2}\eta. \quad (9)$$

$\sigma_{DC}=\sigma$ $(\omega=0,\beta)$ is the electrical conductivity (taken from our resistivity measurements, Fig. 1 [a useful relation is $1\ (\Omega\ \mathrm{cm})^{-1}=4.78\ \mathrm{cm}^{-1}$]) and $\beta=1/kT$. In our analysis of optical conductivities we use the results at $T=80$ K for an easier identification of the phonon sum processes. The frequency $\overline{\omega}$ corresponds to the average between the transverse and the longitudinal-optical mode of a restrahlen band and η, characterizing the strength of the electron-phonon interaction, is the average number of phonons that contribute to the polarization around a localized polaron.[16] Thus, since phonon frequencies are fixed by reflectivity measurements, the only remaining parameter free to fit in each phonon contribution is η.

REFLECTIVITIES AND DISCUSSION

A. $LaFeO_3$

$LaFeO_3$ is a transition $3d$ metal oxide antiferromagnetically ordered at room temperature (Néel temperature, $T_N=740$ K) with Fe^{3+} ions in an orthorhombic environment and with a charge-transfer gap of 2–3 eV.[17] The perovskite distortion comes from the tilting of the octahedra and thus we expect to find several phonon bands in each of the

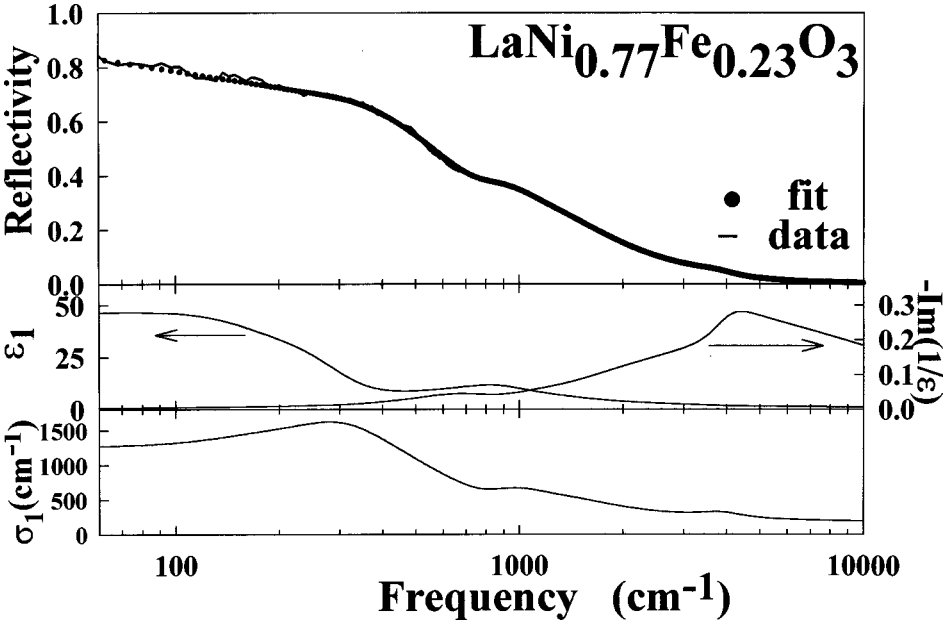

FIG. 10. Infrared reflectivity spectra; ε_1, real part of the dielectric function; $-\mathrm{Im}(1/\varepsilon)$, the imaginary part of the reciprocal of the dielectric function, and σ_1, optical conductivity of $LaNi_{0.77}Fe_{0.23}O_3$ at 80 K.

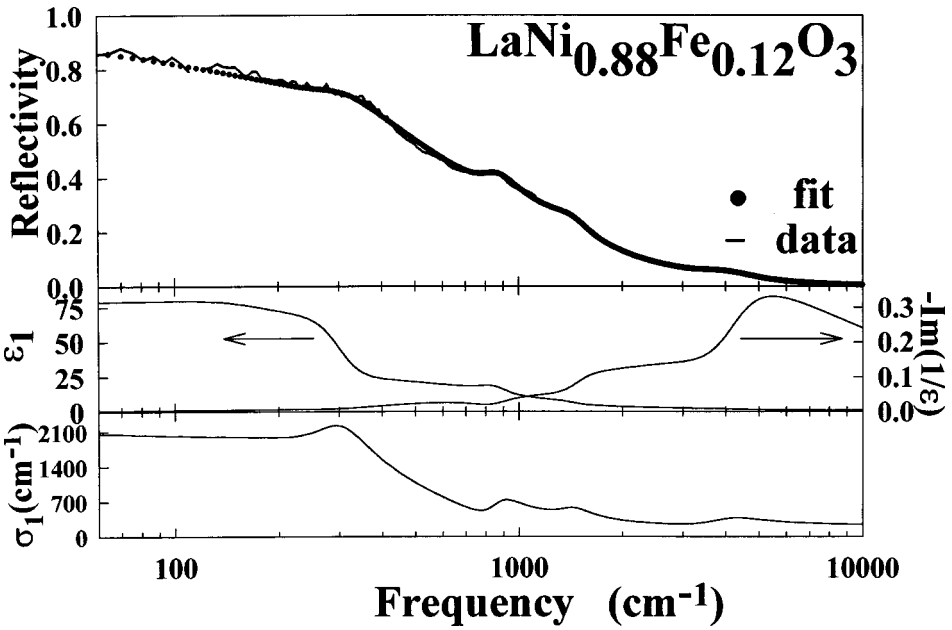

FIG. 11. Infrared reflectivity spectra; ε_1, real part of the dielectric function; $-\mathrm{Im}(1/\varepsilon)$, the imaginary part of the reciprocal of the dielectric function, and σ_1, optical conductivity of $LaNi_{0.88}Fe_{0.12}O_3$ at 80 K.

stretching (650–500 cm^{-1}), bending (200–400 cm^{-1}), and lattice (200–30 cm^{-1}) spectral regions of the ideal cubic structure.

An early infrared transmission measurement for $LaFeO_3$ was reported by Couzi and Houng.[18] More recently, Tajima *et al.*[19] reported a reflectivity spectrum. Although it lacks of sharp features it seems to be in an overall agreement with our band positioning. With an orthorhombic structure belonging to the $D_{2h}^{16}-Pbnm$ space group, and four formula units per unit cell,[20] the total number of zone-center vibrational modes calculated by factor group analysis is[21]

$$\Gamma_{\text{optical}}=7A_g+5B_{1g}+7B_{2g}+5B_{3g}+8A_u+9B_{1u}+7B_{2u}+9B_{3u}, \tag{10}$$

where B_{1u}, B_{2u}, and B_{3u} are the infrared-active species.

Table I shows the phonons that are necessary to obtain an excellent fit to our experimental points (Fig. 3). We found that $LaFeO_3$ behaves truly like an insulator with no anomalies either in the phonon or, at higher frequencies, in the ''electronic'' regions at the temperatures that it was studied.

B. $LaNi_{0.10}Fe_{0.90}O_3$

The introduction of 10% of Ni ions in place of Fe produces mainly a distortion in the bending and stretching band modes without an apparent breakdown of the $\mathbf{k}\cong 0$ selection rule. The fitting parameters, Table I, for the phonon spectrum are essentially the same as in the case of the pure compound. However, as it is shown in Fig. 4 for $x=0.90$, at frequencies higher than the highest breathing vibration, i.e., the longitudinal-optical mode at $\sim 600\ cm^{-1}$, there are weak contributions that we simulate with a broad overdamped band at 2800 cm^{-1}. It grows from interband transitions from new localized states within the $LaFeO_3$ insulating gap and shows itself as a relative increment in the real part of optical conductivity, at about 2900 cm^{-1}.

C. $LaNi_{0.23}Fe_{0.77}O_3$

When we increase the amount of Ni ions to $1-x=0.23$ the number of the states in the insulating gap also increases and consequently, the electronic activity grows in intensity. We see in Fig. 5 that in addition to the overall higher reflectivity in the electronic region there is a feature at 3300 cm^{-1}

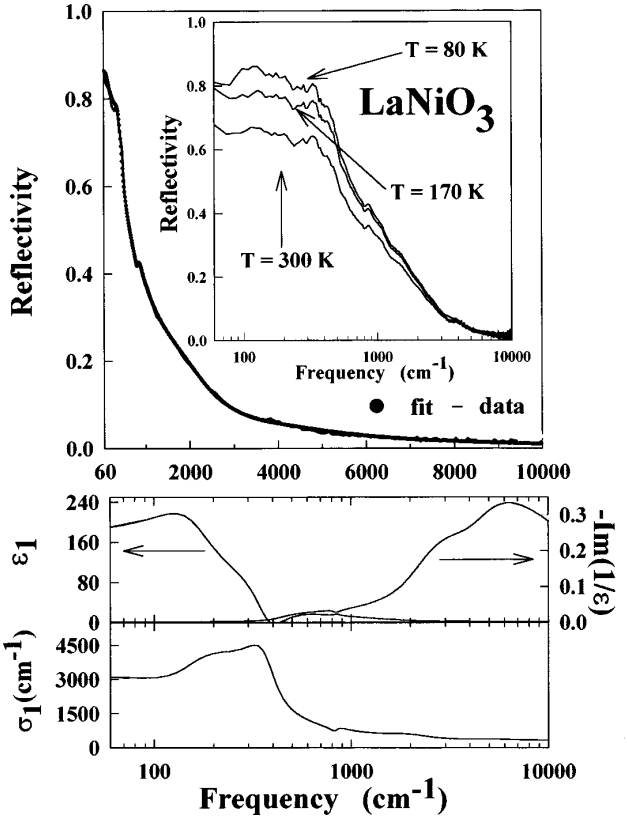

FIG. 12. Infrared reflectivity spectra; ε_1, real part of the dielectric function; $-\mathrm{Im}(1/\varepsilon)$, the imaginary part of the reciprocal of the dielectric function, and σ_1, the real part of the optical conductivity of $LaNiO_3$ at 80 K. The inset shows the reflectivity temperature dependence.

that might be related to an effective relaxation of the $k \cong 0$ selection rule producing a structure in which phonon-assisted processes might also contribute. We note that although the main phonon features for this concentration of Ni ions are the same as in $LaNi_{0.10}Fe_{0.90}O_3$, each band has a smoother profile due to higher damping. The exception is the phonon in which the La vibrates against the $[Ni_{0.23}Fe_{0.77}]O_6$ octahedra at 170 cm^{-1} that keeps and perhaps, increases, its dipole intensity. This is likely another consequence of the disorder in the lattice breaking of the zone-center selection rule and the suggestion, not yet quantitative, of the appearance of a very weak continuum, centered about 200 cm^{-1}, that may be attributed to lattice defects. We locate this band between the lattice mode frequencies involving the La ion against the octahedra and that for the octahedra bending modes.

D. $LaNi_{0.39}Fe_{0.61}O_3$

An incipient continuum is identifiable in $LaNi_{0.39}Fe_{0.61}O_3$ (Fig. 6). We materialize its presence by introducing a Drude term with $\omega_{pl} \cong 512$ cm^{-1} in our dielectric simulation. In addition, we add subbands that contribute to the enhancing of the electronic background beyond 600 cm^{-1}. For this amount of Ni ions the bands roughly delineated at 1500 and 2100 cm^{-1} are assigned to impurity defect transitions. They are similar in nature to those already reported for other distorted perovskite oxides and collectively known as MIR bands. Changes in the dielectric response appear in which the interband-transition scenario starts to switch over towards a picture in which the weight of the spectrum lies at lower frequencies. We note that where in $LaNi_{0.23}Fe_{0.77}O_3$ there was an interband feature centered at ~ 4000 cm^{-1} now we have two lower frequency bands and a precursor of the reflectivity tail that is characteristic in conducting oxides.[22] Here, the few carriers of our semiconducting sample [the number in terms of an electronic effective mass, m^*, is $N \sim 14(m^*/m)10^{16}$] are likely to be strongly localized in the lattice.

E. $LaNi_{0.50}Fe_{0.50}O_3$

Although $LaNi_{0.50}Fe_{0.50}O_3$ is a semiconducting solid solution and its reflectivity does not have a defined plasma edge, the infrared spectrum, Fig. 7, has a tail extending beyond 1 eV showing that its detection does not require that the oxide be metallic. The Drude component, with plasma frequency $\Omega_{pl} \sim 1024$ cm^{-1}, is only incipient. The number of carriers, $N^* \approx 10^{17}$ is the amount expected for a semiconductor [we use $m^* \sim 10$ m, the effective electronic mass determined for $LaNiO_3$ (Ref. 23) to calculate the effective number of carriers N^*]. The optical conductivity has a relative increment at about 4000 cm^{-1} suggesting that extra bands are needed for a good fit and it is interpreted as due to transitions of partially delocalized states in a polaron-related environment. We favor this interpretation because the strong electron-phonon interaction that is inferred in the reflectivity spectrum of this solid solution.

Figure 8 shows that the temperature dependence of reststrahlen bands associated with the main infrared-active phonons for cubic perovskites. As expected for a classical ionic compound[24] they have their damping reduced at the transverse-optical frequencies when the temperature is lowered. In addition, they clearly develop antiresonances near the longitudinal-optical modes. These antiresonances originate in the coupling of carriers with the field that would rise the transverse-longitudinal-optical splitting in purely ionic materials. The ''depths'' of these antiresonances are a qualitative measure of the strength of the electron-phonon interaction in the Fröhlich coupling constant that depends on the electron effective mass and charge; on the low- and high-frequency dielectric constants, and on the longitudinal-optical frequency ω_{LO}.[25,26] We conclude that the reflectivity spectrum of infrared-active phonons in $LaNi_{0.50}Fe_{0.50}O_3$, embedded in a continuous background and with an anomalous temperature-dependent damping near the longitudinal-optical phonons, recreate an environment where polaron behavior and conductivity may be certain. Macroscopically, we trace the origin of that scenario to the highly polarizable lattice[27] created by the oxygen ion since it has polarizabilities strongly dependent on its surroundings[28] and it is known that the O^{2-} ion is unstable in the free state.[29]

On the other hand, we believe that this scenario is common for correlated carriers in oxides. Phonon bands with antiresonances are also found as a reflectivity characteristic of superconductors with high critical temperature, or their parent compounds.[30] These are found in the temperature dependence of phonon spectra for polarization perpendicular to the superconducting **ab**-CuO_2 planes. (For example, see Refs. 31 and 32).

F. $LaNi_{0.63}Fe_{0.37}O_3$

When the replacement of Fe by Ni is increased to $x = 0.37$, the resistivity, Fig. 1, shows that $LaNi_{0.63}Fe_{0.37}O_3$ is semimetallic. The reflectivity spectrum (Fig. 9) exhibits the phonon structure mostly screened while the electrons are likely to be in a strong correlated regime. The dielectric functions is increasingly closer to the ones for other conducting oxides, and in particular, it already suggests the overall response found for high-temperature superconductors in the normal state up to 10 000 cm^{-1} (Ref. 22). We find this behavior in spite of a reverse in the resistivity slope of $LaNi_{0.63}Fe_{0.37}O_3$. It goes from a near linear metallic temperature dependence to one for a low-temperature insulator. It is worth mentioning that we still need extra-Drude bands in the reflectivity fitting in spite of having a stronger and dominant Drude term with $\Omega_{pl} \sim 1875$ cm^{-1}, yielding $N^* \sim 10^{18}$.

G. $LaNi_{0.77}Fe_{0.23}O_3$

$LaNi_{0.77}Fe_{0.23}O_3$ is mostly metallic at 80 K. It has a reflectivity, Fig. 10, that shows a strong tail and may easily be fit with a Drude term, $\Omega_{pl} \sim 3507$ cm^{-1}, $N^* \sim 6 \times 10^{18}$, and extra-Drude bands, assigned to localized defect induced states again, between 600 and 4000 cm^{-1}. This behavior and the resistivity ranging from a metal-like regime to an insulating state may be understood as a change in conductivity reflecting a temperature-dependent enhancement of carrier localization in the lattice.

H. $LaNi_{0.88}Fe_{0.12}O_3$

A truly metallic oxide, i.e., with the reflectivity tending to a near linear dependence with energy in the infrared region is

TABLE II. Fitting parameters for $LaNi_{(1-x)}Fe_xO_3$: the Drude term.

x	ε_∞	Ω_{to} (cm^{-1})	Ω_{lo} (cm^{-1}) Ω_{pl} (cm^{-1})	γ_{to} (cm^{-1}) γ_0 (cm^{-1})	γ_{lo} (cm^{-1}) γ_{pl} (cm^{-1})	S_j (cm^{-2})
		158.7	187.0	18.5	3.5	6.632
		278.8	327.2	62.4	42.8	5.810
		340.7	364.2	39.2	1128.4	0.915
0.50	1.01	365.4	455.4	2164.3	97.0	0.071
		568.9	584.7	24.0	48.9	0.159
		870.7	931.0	406.7	677.9	0.575
		2194.7	4670.5	5718.5	5797.8	3.313
			1024.6	213.6	433.9	
		109.2	238.9	74.7	1397.2	32.719
		358.2	369.6	103.5	124.6	0.557
		497.9	745.6	917.9	125.4	4.339
0.37	1.12	827.7	1266.4	276.9	850.4	0.561
		2060.3	2304.8	1226.2	1957.33	0.205
		3729.6	3818.8	2480.0	4216.3	0.044
			1875.3	1250.6	1071.2	
		160.3	209.1	191.2	245.9	14.73
		297.6	587.7	264.9	1449.0	9.724
0.23	1.02	590.3	707.6	890.9	0.3	0.019
		872.9	1269.2	495.9	975.3	0.603
		1406.3	1511.0	932.5	2048.5	0.041
		3861.2	4044.1	1464.3	1640.8	
			3507.2	922.4	802.6	
		160.3	209.1	171.1	245.9	10.63
		301.9	527.0	144.9	1287.4	6.885
0.12	1.01	535.1	656.8	746.2	10.1	0.067
		856.8	1139.2	216.2	879.4	0.555
		1429.2	1565.6	415.3	1107.4	0.112
		4025.2	4335.9	1835.9	2829.6	0.148
			3421.2	412.3	449.1	
		160.3	185.7	186.43	1700.9	18.277
		222.6	307.1	393.0	253.1	12.904
0.00	1.06	370.9	831.2	181.8	507.1	5.297
		524.3	651.1	263.9	528.6	0.206
		834.1	1102.2	2190.8	1654.8	1.093
		1942.4	3234.7	1820.6	2846.9	1.590
		4124.5	2422.1	2248.0	3712.4	0.034
			3832.9	236.9	444.4	

already found for $x=0.12$ (Fig. 11). Although the number of carriers, $N^* \sim 6\times10^{18}$, deduced from the Drude plasma frequency at ~ 3421 cm^{-1} is about the same as for $x=0.23$ the resistivity is one order of magnitude lower. We nevertheless require the introduction of mid-infrared bands to simulate the existence of regions within the sample in which electron localization varies. The different trend between the optical and transport measurement may reveal the limits of the estimation of conducting carriers by optical means that may be influenced by intergranular resistance.[33]

I. $LaNiO_3$

The spectrum of $LaNiO_3$ (Fig. 12) reflects a relative small increase in the number of effective carriers to $N^* \sim 8\times10^{18}$, having a better defined Drude profile at 80 K. Its metallic behavior was first reported by Goodenough and Raccah[34] based on susceptibility measurements. The Pauli susceptibility of $LaNiO_3$ is independent of temperature (Fig. 2), and earlier neutron scattering measurements showed that there is no magnetic ordering up to 4 K.[35] Its resistivity (Fig. 1), in agreement with that measured by Xu *et al.*,[36] obeys a

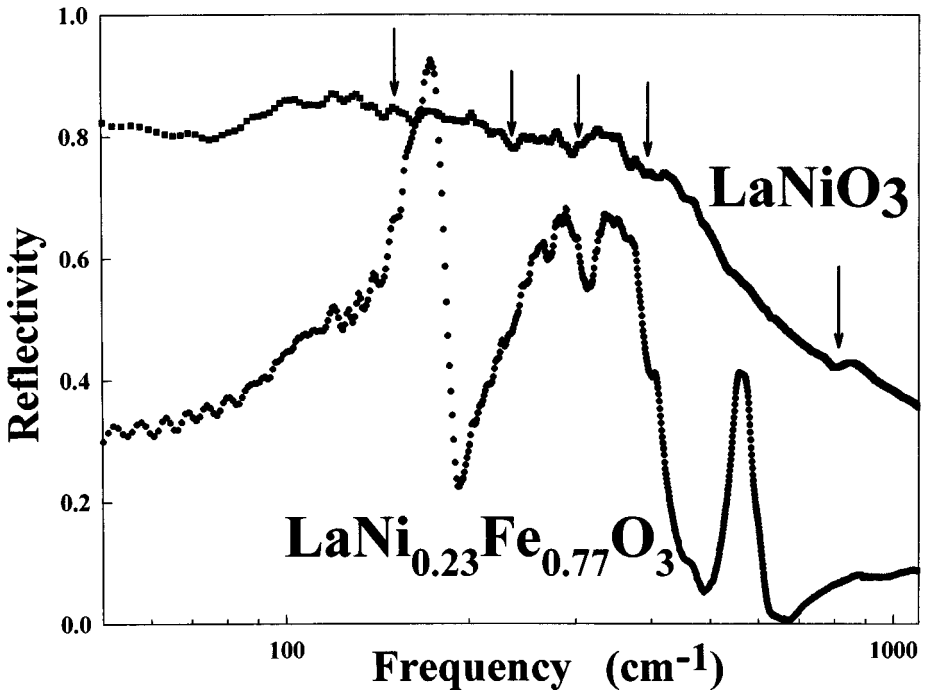

FIG. 13. Far-infrared reflectivity of $LaNiO_3$ and $LaNi_{0.23}Fe_{0.77}O_3$ at 80 K plotted in a semilogarithmic graph. The arrows show the effect of electron-phonon interactions in the reflectivity of $LaNiO_3$.

temperature power law $T^{1.5}$ from $T=80$ to 300 K. From these measurements it was concluded that the $3d$ electrons are highly correlated in this compound.

We find that the infrared reflectivity of $LaNiO_3$, as suggested from its resistivity crossing with that for $x=0.10$, is similar to those for light Fe-doped solid solutions. The inset in Fig. 12 shows that its temperature evolution is indeed the one expected for a metal confirming our results from transport measurements.

The overdamped ''extra-metallic'' bands from 700 to 4000 cm^{-1}, Table II, are similar to those discussed above. Alternatively, the optical conductivity of copper oxides may be decomposed in a normal Drude term, and bands peaking at about 1000 cm^{-1} and at about 5000 cm^{-1} in $Nd_{2-x}Ce_xCuO_4$ (Ref. 37). Thomas *et al.*[38] decomposed the optical conductivity of $YBa_2Cu_3O_{6.1}$, $Nd_2CuO_{4-\delta}$, and $La_2CuO_{4+\delta}$ in the insulating state identifying bands at 1000 cm^{-1}, and another component at 4000 cm^{-1}. Although the number of bands may vary depending on the way chosen for the spectral analysis, we believe that the origin of all that structure in the mid infrared is shared and pinpoints to defects in the oxides.[37,38,39] They are also related to photoinduced bands at about the same frequencies.

In our case doing the analysis directly on the measured reflectivity spectra allows us to identify a reflectivity dip at about 650 cm^{-1} whose origin can be traced to the highest longitudinal-optical symmetric stretching mode. Thus, we find it reasonable to ascribe that band to an effect on localized electrons driven by the phonon breathing motion. All in all, this part of the MIR band complex may be understood as due to localization changes depending on the complexity of the environment encountered by the carrier within the unit cell. Then, our simulation with three bands, non-Drude contributions, in the mid-infrared represent different degrees of localization that do not change significantly as the temperature varies from 300 to 80 K. It should be noticed that this picture is somehow arbitrary since following that line of though we may also justify a two-fluid model replacing some of those extra non-Drude bands with a two-Drude component fit. This allows an equally satisfactory result.

Within a polaronic picture an increment in the amount of Ni dopage is to be thought of as inducing changes in the electron residence time $\tau_{\bullet}$ in a lattice distortion. When that is compared with the lattice vibration $\tau_{\circ}$ the carriers may be considered free for $\tau \sim 10^{-14}$ (Ref. 11). Depending on the energy region of our spectra, the MIR bands may represent different degrees of localization from the one for a large polaron, i.e., a Fröhlich constant $\alpha<5$, to one for a small polaron. Conduction will then be along a phonon-assisted hopping motion (polaron conduction).[40]

An understanding along that interpretation is supported by our analysis of the metallic response of $LaNiO_3$. As is shown in Fig. 13 the weaker substructure in the lattice region should not be dismissed as artifacts from spectral noise. It can be seen that when the reflectivity is compared with an arbitrarily chosen far-infrared spectrum of one of our insulators, the relatively weak absorption dips have a direct correspondence with the frequencies of the longitudinal-optical phonons of the principal perovskite vibrations. Although our end sample behaves in a metallic way (inset, Fig. 12), its reflectivity shows unquestionable marks of strong electron-phonon interactions that have to be related with the real mechanism for conductivity. We believe that this is the most likely explanation of the relative high effective electron mass, $m^*=10m$, and of the departure of the resistivity from the linear temperature dependence.

We trace polaron formation to the fact that when $LaNiO_3$ is prepared it is sensitive to oxygen pressures at high temperatures. Ni^{3+} can be partially reduced in air to Ni^{2+} to produce oxygen vacancies which makes realistic, as pointed out at the beginning of this article, that the resulting compound be always thought of as

$$La(Ni^{2+}{}_m, N^{3+}{}_n)O_{3-\delta}, \quad m+n=1, \tag{11}$$

with oxygen defects (δ) providing grounds for electron localization. We note that Sanchez *et al.* have recently shown that

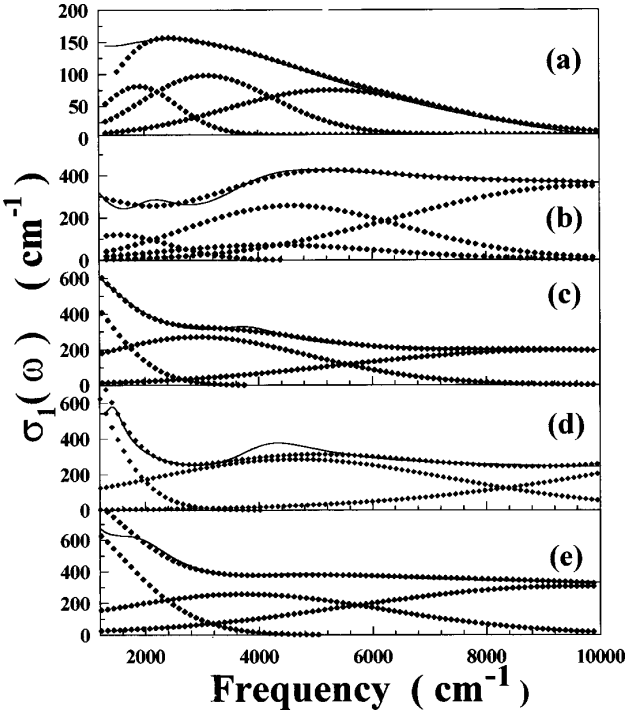

FIG. 14. Optical conductivity of $LaNi_{1-x}Fe_xO_3$ $x=0.50$ (a), 0.37 (b); 0.23 (c), 0.12 (d), 0.00 (e) at 80 K. Full line upper traces are optical conductivities drew from their respective reflectivities. The superposing dots are the estimates using Eq. (6). Individual Gaussians in dot traces correspond to different phonon contributions discussed in the text.

antiferromagnetism and the metal-insulator phase transition may be induced in oxygen-deficient $LaNiO_3$ (Ref. 40).

ANALYSIS OF THE OPTICAL CONDUCTIVITY

In the last section we have already shown the overall evolution of the optical conductivities deduced from our reflectivity spectra and we hinted to evidence for polaron formation. Here we give a closer look at our results in the 1200–10 000 cm^{-1} spectral region doing an analysis of the data in terms of Reik's small polaron picture [Eq. (6)]. Between 600 and 1200 cm^{-1} we expect a mixture of contributions due to polarons and to the two-phonon density of states.

In the analysis we allow, ϖ the average frequency, and η, characterizing the strength of the electron-phonon interaction, to vary freely in the fit. We then compare these results with frequency-dependent experimental data.

A good starting point for our discussion is the insulator spectra of $LaNi_{0.50}Fe_{0.50}O_3$, Fig. 8, where, in addition to the characteristic tail, there are three main bands, nominally, lattice, antisymmetric, and symmetric stretching phonons. These have temperature-dependent strong antiresonances implying distinctive electron-phonon interactions for each phonon group. We found that to cover the complete spectral range up to 10 000 cm^{-1} one simply needs to consider three independent contributions of the type described in Eq. (6). The excellent fit achieved in this fashion is shown in Fig. 14(a). The parameters for $x=0.50$ are in Table III. We also see that in spite of omiting an explicit correlation between the three contributions, the frequencies from the fit are in remarkable agreement with the experimental ones and, as expected the electron-phonon parameters η_j $(j=1,2,3)$ are in the very strong range.

When the number of carrier increases, as for $x=0.37$, 0.23, and 0.12, we found that the character of the phonon contributions for the same spectral range changes accordingly with theory.[15] Now the result of the first-order fit shows ϖ at a frequency that is identified as that for the average phonon in the mixed system. The rest of the conductivity spectrum, as the frequency increases, originates in main contributions from densities of states as overtones and third-order phonon-sum processes (an estimation of these may be visualized by self-convoluting the one-phonon density of states. This results in the overtone density of states, and convoluting this with the former one obtains the third-order term). Table III shows the agreement with experimental frequencies (between brackets) taken from Table II. The number of phonons that form the polaron cloud, η, increases as the phonon order increases. It is interesting to stress again that no correlation of any kind has been introduced in the fit

TABLE III. Parameters of the small polaron theory for $LaNi_{(1-x)}Fe_xO_3$. The values between parentheses are phonon frequency averages from Table II.

x	η_1	ϖ_{ph1} (cm^{-1})	η_2	ϖ_{ph2} (cm^{-1})	η_3	ϖ_{ph3} (cm^{-1})
0.50	12.6	174.1 (172.5)	11.0	345.4 (381.4)	10.6	560.3 (571.7)
			9.8	990.0		
0.37	5.4	316.5 (386.3)	8.2	677.6	12.8	1395.0
0.23	3.6	369.1 (428.0)	5.7	752.7	8.9	1288.3
0.12	2.9	405.0 (401.2)	6.2	1035.2	11.9	1820.0
0.00	3.3	525.9 (587.0)	5.6	975.9	8.60	1399.7

and that the parameters were left to vary freely. We also note, however, that the model in the finite-temperature approximation used here is unable to reproduce sharper features as in the band at $\sim 4000\ \mathrm{cm}^{-1}$. In this one, for $x = 0.37$, we found that a small asymmetry may be approached assuming two slightly different Gaussian contributions that can be understood as essentially reflecting the mixed system character of our compound. They would represent environments with different relaxation times τ.

When the optical conductivity of the pure compound, $LaNiO_3$, is analyzed an excellent fit is achieved. As suggested in Ref. 16, now, it is only necessary to take into account the highest vibrational band, in our case, $\varpi \sim 587\ \mathrm{cm}^{-1}$ for breathing phonons that is in very good agreement with the experimental average from transverse- and longitudinal-optical frequencies given in the Table II. In this case the calculated fitted frequencies at $\sim 975.9\ \mathrm{cm}^{-1}$ and $\sim 1339.7\ \mathrm{cm}^{-1}$ are assigned to overtone and third-order-sum processes, respectively.

CONCLUSIONS

Summarizing, we have measured the far- and midinfrared reflectivity spectra of $LaNi_{(1-x)}Fe_xO_3$ $(0.00 \leqslant x \leqslant 1.00)$. The spectra of these single phase solid solutions show for light Ni-doping interband transitions due to defects in the lattice in addition to bands assigned to distorted perovskite phonons. An incipient Drude term emerges in the reflectivity spectrum of $LaNi_{0.39}Fe_{0.61}O_3$ together with subbands that contribute to the electronic background. For these concentrations it is found the development of the reflectivity tail characteristic of all conducting oxides and evidence of strong electron-phonon interactions is detected as antiresonances near longitudinal-optical mode frequencies.

While there are no special reflectivity features in the insulator-metal transition, at $x \sim 0.30$, a metal oxide spectrum is measured for $x = 0.23$ where phonons are mostly screened. An absorption dip that is traced to the perovskite symmetric stretching longitudinal mode at about $650\ \mathrm{cm}^{-1}$ is evidence of electron-phonon interactions in our solid solutions, even when their numbers of effective carriers are those as for a metal. This characterization is supported by the observation of weak reflectivity dips in $LaNiO_3$ that have a direct correspondence to longitudinal-optical mode frequencies in the insulating phases of our series. We also show that the small-polaron picture in Refs. 12 and 16 gives a consistent interpretation of our experimental optical conductivity. In agreement with Reik and Heese,[12] we conclude that the contribution of diagonal processes to the optical conductivity in the infrared seems to be negligible.

We believe that our conclusions may be relevant toward understanding the reflectivity spectrum of metal oxides in general because the conductivity in $LaNiO_3$ is three dimensional. This is in contrast with other perovskite-derived systems, as in the case of the CuO_2 planes of high-temperature superconductors, that are metals in one or two dimensions. Being three dimensional avoids the argument of misinterpreting possible band features in the metallic **a**-**b** reflectivity plane as due to band leakages of the mostly unscreened phonon activity along the **c** direction.[31,32]

From the extraordinary number of oxides that show superconductivity, our measurements suggest that the reason for any of these materials becoming superconductor may reside in the strength that a particular interaction would allow, say, bipolaron formation,[41] and thus pair formation. Our conducting solid solutions are perhaps too ionic and with too low of a carrier density to sustain superconductivity. It is known that the larger effective masses of the nickelates exceed those of the cuprates[42] and thus the condensation tends to be polaronic.[41]

ACKNOWLEDGMENTS

This research has been partially supported by a Grant PID 3956/92 of the National Research Council of Argentina (CONICET) and a grant of the CONICET to centro CEQUINOR and INFIQC. N.E.M. wants to thank the Organization of the American States for a support that allowed him a stay at National Synchrotron Light Source, Brookhaven National Laboratory, Upton, New York, U.S.A. where some of the calculations were made. Thanks are also due to G. Williams for the hospitality at the NSLS. R.E.C. wishes to acknowledge financial support from the Secretaría de Ciencia y Técnica of the Universidad de Córdoba, the Fundación Antorchas and CONICOR.

[1] Reported work on related systems may be found in Y. Terasaki, T. Nakahashi, A. Maeda, and K. Uchinokura Phys. Rev. B **43**, 551 (1991); G. A. Thomas, D. H. Rapkine, S. L. Cooper, S.-W. Cheong, A. S. Cooper, L. F. Schneemeyer, and J. V. Waszczak, *ibid.* **45**, 2474 (1992); D. A. Crandles, T. Timusk, J. D. Garrett, and J. E. Greedan, *ibid.* **49**, 16 207 (1994); T. Ido, K. Magoshi, H. Eisaki, and S. Uchida, *ibid.* **44**, 12 094 (1991).

[2] G. Binnig, A. Baratoff, H. E. Honig, and J. G. Bednorz, Phys. Rev. Lett. **45**, 1352 (1980).

[3] P. Calvani, M. Capizzi, F. Donato, S. Lupi, P. Maselli, and D. Peschiaroli, Phys. Rev. B **47**, 8917 (1993).

[4] H. G. Reik, Z. Phys. C **203**, 346 (1967); D. M. Eagles and P. Lalousis, J. Phys. C **17**, 655 (1984).

[5] J. M. D. Tascón, S. Mendioroz, and L. Gónzalez Tejuca, Z. Phys. Chem. (Munich) **124**, 109 (1981).

[6] P. Odier, Y. Nigara, J. Coutures, and M. Sayer, J. Solid State Chem. **56**, 32 (1985).

[7] J. Takahashi, T. Toyoda, T. Ito, and M. Takatsu, J. Mater. Sci. **25**, 1557 (1990).

[8] A. E. Goeta, G. F. Goya, R. C. Mercader, G. Punte, H. Falcon, and R. Carbonio, Hyperfine Interact. **90**, 371 (1994).

[9] H. Falcon, A. E. Goeta, G. Punte, and R. E. Carbonio (unpublished).

[10] N. Y. Vasanthacharya, P. Ganguly, and C. N. R. Rao, J. Solid State Chem. **53**, 140 (1984).

[11] P. Ganguly, N. Y. Vasanthacharya, and C. N. R. Rao, J. Solid State Chem. **54**, 400 (1984).

[12] H. G. Reik and D. Heese, J. Phys. Chem. Solids **28**, 581 (1967).

[13] T. Kurosawa, J. Phys. Soc. Jpn. **16**, 1208 (1961).
[14] F. Gervais, J. L. Servoin, A. Baratoff, J. G. Bednorz, and G. Binnig, Phys. Rev. B **47**, 8187 (1993).
[15] T. Holstein, Ann. Phys. (N.Y.) **8**, 343 (1959).
[16] R. Mühlstroh and H. G. Reik, Phys. Rev. **162**, 703 (1967).
[17] A. E. Bocquet, A. Fujimori, T. Mizokawa, T. Saitoh, H. Namatame, S. D. Suga, N. Kimizuka, Y. Takeda, and M. Takano, Phys. Rev. B **45**, 1561 (1992).
[18] M. Couzi and P. Van Houng, J. Chim. Phys. **69**, 1339 (1972).
[19] S. Tajima, A. Masaki, S. Uchida, T. Matsuura, K. Fueki, and S. Sugai, J. Phys. C **20**, 3469 (1987).
[20] F. S. Galasso, *Structure, Properties and Preparation of Perovskite-like Compounds* (Pergamon, New York, 1969).
[21] M. Reedyk, D. A. Crandles, M. Cardona, J. D. Garret, and J. E. Greedan, Phys. Rev. B **55**, 1442 (1997).
[22] I. Bozovic, J. H. Kim, J. S. Harris, C. B. Eom, J. M. Phillips, and J. T. Cheung, Phys. Rev. Lett. **73**, 1436 (1994).
[23] K. P. Rajee, G. V. Shivashankar, and A. K. Raychaudhuri, Solid State Commun. **79**, 591 (1991). Also, K. Sreedhar, J. M. Honig, M. Darwin, M. McElfresh, P. M. Shand, J. Xu, B. C. Crooker, and J. Spalek, Phys. Rev. B **46**, 6382 (1992).
[24] S. S. Mitra, in *Optical Properties of Solids*, edited by S. Nudelman and S. S. Mitra (Plenum, New York, 1969).
[25] A. J. Bosman and H. J. Van Daal, Adv. Phys. **19**, 1 (1970).
[26] A. A. Shanenko, M. A. Smondyrev, and J. T. Devreese, Solid State Commun. **98**, 1091 (1996).
[27] H. Bilz, G. Benedek, and A. Bussmann-Holder, Phys. Rev. B **35**, 4840 (1987).
[28] G. R. Tessmann, A. H. Kohn, and W. Shockley, Phys. Rev. **92**, 890 (1953).
[29] R. F. Prat, Phys. Rev. A **6**, 1735 (1972).
[30] T. Timusk, C. D. Porter, and D. B. Tanner, Phys. Rev. Lett. **66**, 663 (1991).
[31] C. C. Homes, T. Timusk, D. A. Bonn, R. Liang, and W. N. Hardy, Physica C **254**, 265 (1994).
[32] S. Uchida, K. Tamasaku, and S. Tajima, Phys. Rev. B **53**, 14 558 (1996).
[33] K. H. Kim, J. Y. Gu, H. S. Choi, D. J. Eom, J. H. Jung, and T. W. Noh, Phys. Rev. B **55**, 4023 (1997).
[34] B. Goodenough and P. M. Raccah, J. Appl. Phys. **36**, 1031 (1965).
[35] W. E. Koehler and E. O. Wollan, J. Phys. Chem. Solids **2**, 100 (1957).
[36] X. Q. Xu, J. L. Peng, Z. L. Peng, Z. Y. Li, H. L. Ju, and R. L. Greene, Phys. Rev. B **48**, 1112 (1993).
[37] S. Lupi, P. Calvani, M. Capizzi, P. Maseli, W. Sadowski, and E. Walker, Phys. Rev. B **45**, 12 470 (1992).
[38] G. A. Thomas, D. H. Rapkine, S. L. Cooper, L. F. Schneemeyer, and J. V. Waszcak, Phys. Rev. B **48**, 4043 (1996).
[39] P. Calvani, M. Capizzi, S. Lupi, P. Maselli, A. Paolone, and P. Roy, Phys. Rev. B **53**, 2756 (1996); C. M. Foster, A. J. Heeger, G. Stucky, and N. Herron, Solid State Commun. **71**, 945 (1989); P. Calvani and S. Lupi, *ibid.* **85**, 665 (1993).
[40] R. D. Sanchez, M. T. Causa, A. Caneiro, A. Butera, M. Vallet-Regi, M. J. Sayagués and J. González-Calbet, F. Garcia-Sanz, and J. Rivas, Phys. Rev. B **54**, 16 574 (1996).
[41] D. Emin, Phys. Rev. B **48**, 13 691 (1993).
[42] X.-X. Bi and P. C. Eklund, Phys. Rev. Lett. **70**, 2635 (1993).